

## Fate of soliton matter upon symmetry-breaking ferroelectric order

K. Sunami <sup>1,\*</sup>, R. Takehara <sup>1</sup>, A. Katougi <sup>1</sup>, K. Miyagawa <sup>1</sup>, S. Horiuchi <sup>2</sup>, R. Kato <sup>3</sup>,  
T. Miyamoto <sup>4</sup>, H. Okamoto <sup>4,5</sup> and K. Kanoda <sup>1,†</sup>

<sup>1</sup>Department of Applied Physics, University of Tokyo, Bunkyo-ku, Tokyo 113-8656, Japan

<sup>2</sup>Research Institute for Advanced Electronics and Photonics, National Institute of Advanced Industrial Science and Technology, Tsukuba, Ibaraki 305-8565, Japan

<sup>3</sup>Condensed Molecular Materials Laboratory, RIKEN, Wako, Saitama 351-0198, Japan

<sup>4</sup>Department of Advanced Materials Science, University of Tokyo, Kashiwa, Chiba 277-8561, Japan

<sup>5</sup>AIST-UTokyo Advanced Operando-Measurement Technology Open Innovation Laboratory, National Institute of Advanced Industrial Science and Technology, Chiba 277-8568, Japan



(Received 20 July 2020; revised 15 February 2021; accepted 2 April 2021; published 16 April 2021)

In a one-dimensional (1D) system with degenerate ground states, their domain boundaries, dubbed solitons, emerge as topological excitations often carrying unconventional charges and spins; however, the soliton excitations are vital in only the nonordered regime. Then a question arises: How do the solitons conform to a three-dimensional (3D) ordered state? Here, using a quasi-1D organic ferroelectric, tetrathiafulvalene-*p*-chloranil (TTF-CA), with degenerate polar dimers, we pursue the fate of spin-soliton charge-soliton composite matter in a 1D polar-dimer liquid upon its transition to a 3D ferroelectric order by resistivity, nuclear magnetic resonance (NMR), and nuclear quadrupole resonance (NQR) measurements. We demonstrate that the soliton matter undergoes neutral spin-spin soliton pairing and spin-charge soliton pairing to form polarons, coping with the 3D order. Below the ferroelectric transition, the former contributes to the magnetism through triplet excitations, which rapidly fade out on cooling, whereas the latter carries electrical current with paramagnetic spins that more moderately decrease with temperature. The nearly perfect scaling between NMR and NQR relaxation rates in the ferroelectric phase evidences that spin carriers diffuse with lattice distortion, namely, in the form of polarons. From the combined analyses of conductivity and NMR relaxation rate, we derive the excitation energies of polaron excitations and diffusion. Our results reveal the whole picture of soliton matter that condenses into the 3D ordered state.

DOI: [10.1103/PhysRevB.103.134112](https://doi.org/10.1103/PhysRevB.103.134112)

### I. INTRODUCTION

Coupling between the charge, spin, and lattice in solids gives rise to emergent low-energy excitations, which appear as solitons with a topological nature in one-dimensional (1D) systems with degenerate ground states [1,2]. The quasi-1D organic donor-acceptor complex tetrathiafulvalene-*p*-chloranil (abbreviated TTF-CA) [Fig. 1(a)] offers an exclusive ground for the physics of charge solitons and spin solitons [3–14]. TTF-CA is in the neutral phase at ambient temperature and pressure; however, pressurizing or cooling induces a neutral-to-ionic (NI) transition [15–21] with a collective charge transfer from TTF to CA. The ionicity  $\rho$  defined by  $\text{TTF}^{+\rho}\text{-CA}^{-\rho}$ , which takes a partial value ( $0 < \rho < 1$ ) due to the transfer integral between the highest occupied molecular orbital (HOMO) of TTF and lowest unoccupied molecular orbital (LUMO) of CA, changes from 0.3 (neutral) to 0.6–0.7 (ionic) [22–27]. The schematic phase diagram is shown Fig. 1(b). At low temperatures [the green-colored region in Fig. 1(b)], the ionic state is accompanied by a lat-

tice dimerization (donor-acceptor pairing) due to the Peierls or spin-Peierls instability [28–30], yielding a nonmagnetic symmetry-breaking electronic ferroelectric ( $I_{\text{ferro}}$ ) phase taking either of two degenerate dimerization patterns [31,32]. Indeed, in the  $I_{\text{ferro}}$  phase at ambient pressure, the spontaneous electric polarization is observed [32], indicative of the emergence of the three-dimensional (3D) ferroelectric dimer order. This order melts into a polar dimer liquid upon entering a paraelectric ionic ( $I_{\text{para}}$ ) phase at high temperatures above  $\sim 9$  kbar [the orange-colored region in Fig. 1(b)] [21,33,34].

In the  $I_{\text{para}}$  phase, the space inversion symmetry is globally preserved but locally broken [35,36] such that  $S = 1/2$  spin solitons and spinless charge solitons [3,5,6] are thermally excited to interrupt the global order and generate oppositely polarized dimer domains along the 1D chains, which we call the “1D polar-dimer liquid” [Fig. 1(c)]. At 14 kbar and at ambient temperature, for example, the spin-soliton density is 1 per 10–25 donor-acceptor pairs, as revealed by a recent nuclear magnetic resonance (NMR) study [13], whereas the charge-soliton density is 1 per  $\sim 100$  donor-acceptor pairs according to an analysis of a transport experiment described later in detail, although direct and microscopic evidence for the charge solitons remains to be seen. Soliton matter composed of spin solitons (majority) and charge solitons

\*sunami@mdf2.t.u-tokyo.ac.jp

†kanoda@ap.t.u-tokyo.ac.jp

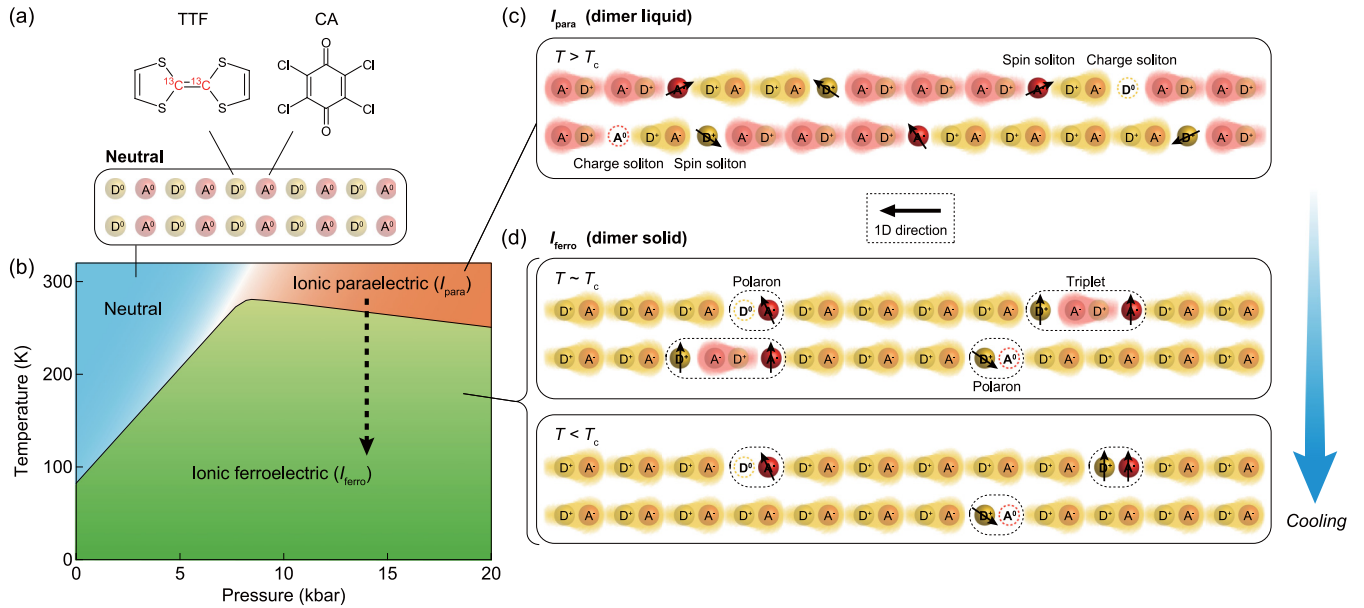


FIG. 1. Phase diagram and spin and charge excitations in TTF-CA. (a) Molecular structures of TTF and CA. The central double-bonded carbon atoms in the TTF molecule are enriched by  $^{13}\text{C}$  isotopes for  $^{13}\text{C}$  NMR measurements. The neutral state ( $\rho = 0$  for simplicity) is illustrated at the bottom, where D and A represent the donor and acceptor molecules, TTF and CA, respectively. (b) Pressure-temperature phase diagram of TTF-CA. The dashed arrow indicates the trace of measurements in the present study. Illustrations of spin and charge excitations in the ionic (c) paraelectric and (d) ferroelectric phases of TTF-CA ( $\rho = 1$  for simplicity), respectively.

(minority) resides in the  $I_{\text{para}}$  phase. An issue of profound interest that has yet to be addressed in soliton physics is what happens in the soliton matter upon entering a 3D ordered phase, where free-soliton excitations are not allowed [37] and the soliton matter is unable to preserve the pristine state [Fig. 1(d)]. The soliton physics has been intensively studied in the conducting polymer, polyacetylene [1], but it does not show the 3D long-range order. Thus, how the free solitons conform to the long-range ordered phase can be addressed only in the present system showing the symmetry-breaking transition from the soliton matter to the 3D ferroelectric. The present study gives a solution to this fundamental issue by investigating TTF-CA under temperature variation across the  $I_{\text{para}}$  and  $I_{\text{ferro}}$  phases through electrical conductivity,  $^{13}\text{C}$  NMR, and  $^{35}\text{Cl}$  nuclear quadrupole resonance (NQR) measurements probing the charge, spin, and lattice, respectively.

## II. EXPERIMENT

For  $^{13}\text{C}$  NMR measurements, we synthesized  $^{13}\text{C}$ -enriched TTF molecules, in which the central double-bonded carbon atoms are labeled by  $^{13}\text{C}$  isotopes with a 99% concentration in the method described in Ref. [13]. Both  $^{13}\text{C}$ -enriched and nonenriched single crystals of TTF-CA were prepared by a cosublimation method. Hydrostatic pressure of 14 kbar was applied to the sample using a nonmagnetic BeCu clamp-type cell (for  $^{13}\text{C}$  NMR and  $^{35}\text{Cl}$  NQR) and a BeCu/NiCrAl dual-structured one (for electrical conductivity measurement) with Daphne 7373 oil as the pressure medium. Electrical conductivity was measured with electrical currents applied along the  $a$  axis (1D direction) of a single crystal by the four-terminal method. The  $^{13}\text{C}$  NMR and  $^{35}\text{Cl}$  NQR measurements were

conducted under an external magnetic field of 8 T directed to the  $a$  axis and under zero field, respectively. The signals of nuclear magnetization were obtained using the solid-echo pulse sequence for  $^{13}\text{C}$  NMR and the spin-echo pulse sequence for  $^{35}\text{Cl}$  NQR. The nuclear spin-lattice relaxation rate is determined by fitting the single-exponential function to the relaxation curve of nuclear magnetization.

## III. RESULTS

### A. $^{13}\text{C}$ NMR

First, we conducted the  $^{13}\text{C}$  NMR measurements with temperature varied across the ferroelectric transition under a pressure of 14 kbar [Figs. 2(a)–2(d)]. At every temperature studied,  $^{13}\text{C}$  NMR spectra have two peaks [Fig. 2(a)] that arise from nuclear dipolar interactions between the central  $^{13}\text{C}$  sites. As temperature is lowered, the spectral shift decreases with a clear kink at a transition temperature,  $T_c \sim 270$  K, in accordance with the previous NQR result [21], and saturates to the value of 82 ppm [Fig. 2(b)]. The spectral shift is the sum of the spin shift  $S$ , proportional to the spin susceptibility, and the chemical shift caused by the orbital motion of electrons. The  $I_{\text{ferro}}$  phase is nonmagnetic due to the spin-singlet formation [7,13], so that we take the saturated value, 82 ppm, as the chemical shift. The plot of  $S$  (equal to the observed shift minus 82 ppm) multiplied by temperature  $T$  vs  $1/T$  [Fig. 2(d)] is well characterized by  $TS \propto \exp(-\Delta_s/k_B T)$  with a spin excitation gap  $\Delta_s$  of 3240 K for  $200 \text{ K} < T < T_c$ , where  $k_B$  is the Boltzmann constant. Conventional spin-Peierls systems are known to hold relationships between  $T_c$  and the singlet-triplet gap  $\Delta$ ,  $\Delta/k_B T_c \sim 1.76$  (the BCS relationship) or 2.47 (obtained with a bosonization method [38]). The present value,

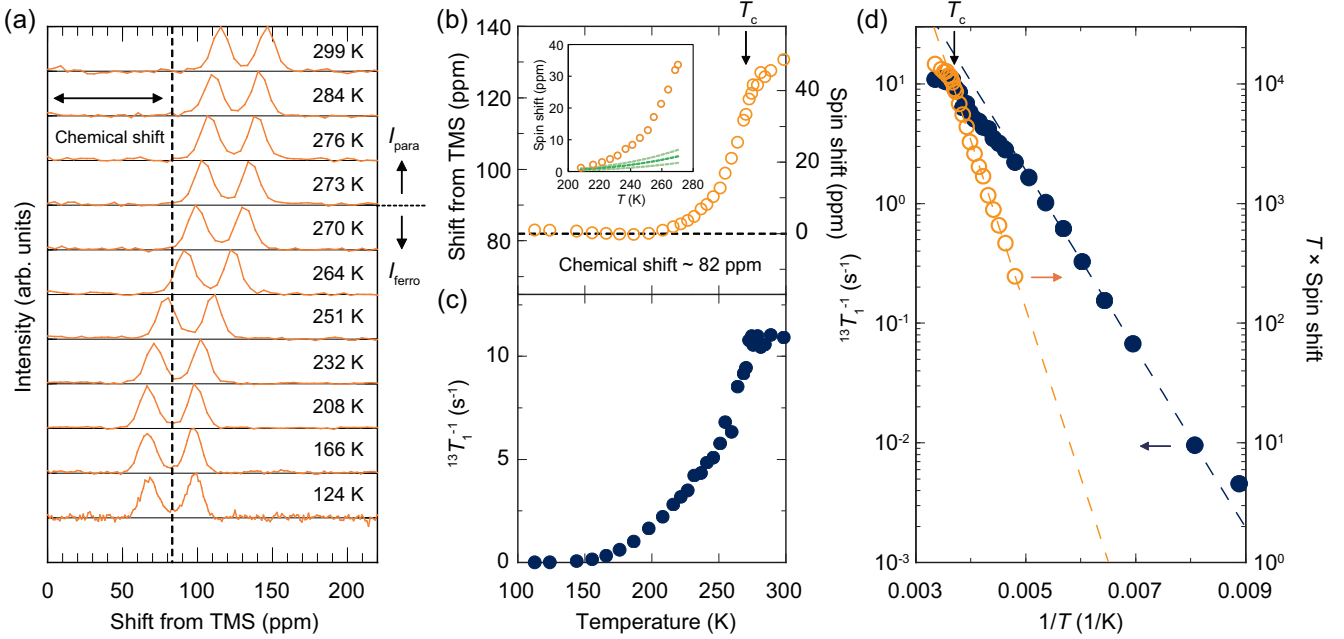


FIG. 2.  $^{13}\text{C}$  NMR spectra, shift, and relaxation rate of TTF-CA. (a) Temperature dependence of  $^{13}\text{C}$  NMR spectra at 14 kbar. The doublet structure arises from the  $^{13}\text{C}$ - $^{13}\text{C}$  nuclear dipolar coupling, and the NMR shift is given by the midpoint of the doublet. The shift origin corresponds to the resonance frequency of TMS (tetramethylsilane). (b) Plot of the midpoint of the doublet as a function of temperature. Left and right axes represent the total shift and the spin shift [total shift – chemical shift (82 ppm)], respectively. Inset: Close-up of the behavior near  $T_c$ . Estimates of the polaron contribution to spin shift are indicated by three green lines (upper and lower limits and their median; see text for the details of the estimation). (c) Temperature dependence of the  $^{13}\text{C}$  NMR spin-lattice relaxation rate  $^{13}T_1^{-1}$  at 14 kbar. (d) Comparison between  $^{13}T_1^{-1}$  (blue solid circles; left axis) and  $T$  times spin shift (orange open circles; right axis) plotted against inverse temperature. The blue dashed line is a fit of the single-exponential function to  $^{13}T_1^{-1}$  in the range  $120 < T < 200$  K. The orange dashed line is a fit of the single-exponential function to  $T$  times spin shift in the range  $200 \text{ K} < T < T_c$ .

$\Delta_s/k_B T_c$  is  $\sim 12$ , is too large for the conventional spin-Peierls picture for the 1D Heisenberg spins. Indeed, the  $I_{\text{para}}$  phase carries mobile spin and charge solitons, qualitatively different from the conventional paramagnetic phases [13,14].

In the  $I_{\text{ferro}}$  phase below  $T_c$ , the soliton excitations should be in pairs not to violate the 3D ferroelectric order, and thus,  $\Delta_s$  of 3240 K characterizes the excitations of the triplet-type neutral spin soliton-antisoliton pairs, which are determined by the exchange interaction between them.

An unconventional feature of spin excitations is also captured by the  $^{13}\text{C}$  nuclear spin-lattice relaxation rate  $^{13}T_1^{-1}$ , which is nearly independent of temperature above  $T_c$  but decreases below  $T_c$  with a kink at  $T_c$  as in  $S$  [Fig. 2(c)]. The activation plot of  $^{13}T_1^{-1}$  exhibits an exponential decrease characterized by a gap value of  $\Delta_{T_1^{-1}} = 1720$  K defined by  $T_1^{-1} \propto \exp(-\Delta_{T_1^{-1}}/k_B T)$  in  $120 < T < 200$  K, whereas the variation of  $^{13}T_1^{-1}$  is gradual in  $200 \text{ K} < T < T_c$ , where the slope of the activation plot of  $^{13}T_1^{-1}$  is much less than that of  $S$  with  $\Delta_s = 3240$  K [Fig. 2(d)]. In the conventional singlet-triplet excitations, the spin excitation gaps in  $S$  and  $T_1^{-1}$  should not significantly differ [39]; for the spin-Peierls case, the activation energy of  $T_1^{-1}$  is theoretically predicted to be twice that of  $S$  in  $T \ll \Delta/k_B$  due to the indirect three-magnon process [40]. In TTF-CA, however, the observed moderate decrease of  $^{13}T_1^{-1}$  is totally unexplainable by this process, suggesting the presence of another form of spin excitations below  $T_c$ . If a spin soliton and a charge soliton

are bound to form a “polaron” with an elementary charge and a spin 1/2, which is the similar-type excitation discussed in conducting polymers [1], it can be excited and carry charges and spins without violating the ferroelectric dimer order in the  $I_{\text{ferro}}$  phase [Fig. 1(d)]. As we discuss in Sec. IV, the polaron excitation is a major contributor to  $^{13}T_1^{-1}$  except near  $T_c$ , whereas the triplet excitation of bound spin soliton pairs is so to  $S$  near  $T_c$ .

## B. $^{35}\text{Cl}$ NQR

Next, to reveal the profiles of lattice dimerization and fluctuations, we measured the  $^{35}\text{Cl}$  NQR spectra and spin-lattice relaxation rate  $^{35}T_1^{-1}$  at 14 kbar. As shown in Figs. 3(a) and 3(b), the NQR line splits below  $T_c$ , indicative of the lattice symmetry breaking in the  $I_{\text{ferro}}$  phase [21,41,42], where the inversion center on the CA molecule is lost [31]. The order parameter of the ferroelectric order is the magnitude of polarization, which is reasonably assumed to be proportional to the strength of the lattice dimerization detected by the NQR line splitting. The line splitting width that sharply rises at  $T_c$  keeps increasing down to  $\sim 200$  K, albeit gradually below 250 K [see Fig. 3(c)]. The  $I_{\text{para}}$  phase above  $T_c$  results from the excitations of free solitons, which interfere with the ferroelectric long-range order and generate domains with opposite polarizations, as shown in Fig. 1(c). Ferroelectric order from such a state is attained by an imbalance between the volume fractions of oppositely polarized domains and, in terms of

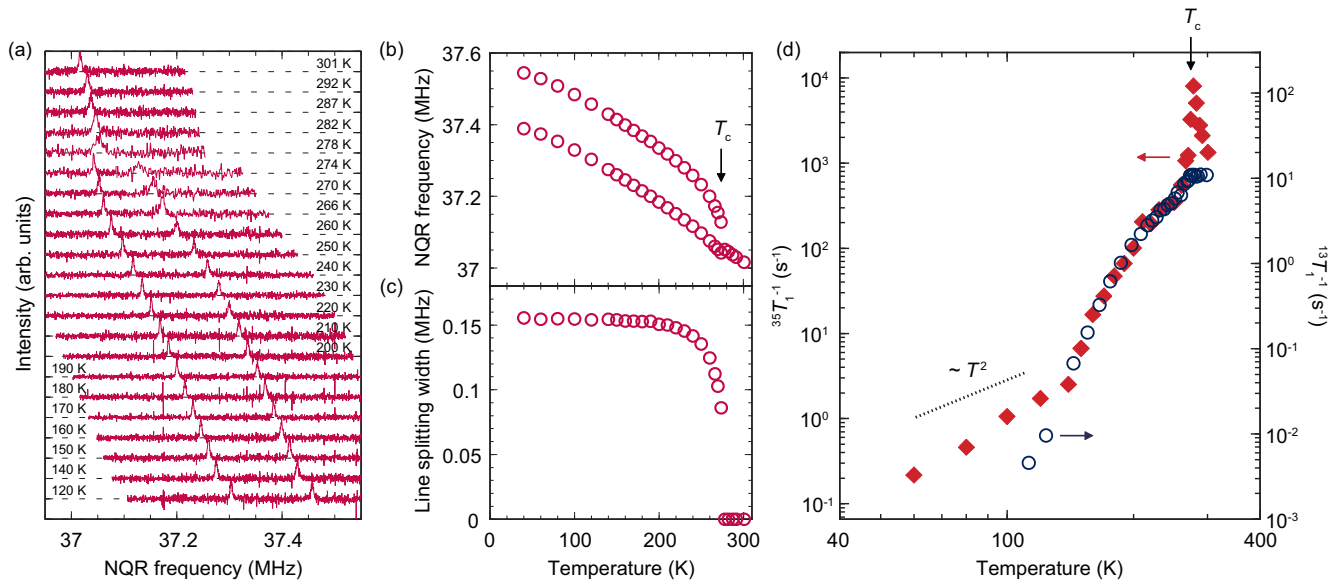


FIG. 3.  $^{35}\text{Cl}$  NQR spectra, frequency, and relaxation rate of TTF-CA. Temperature dependence of (a)  $^{35}\text{Cl}$  NQR spectra and (b) frequency at 14 kbar. (c) Plot of line splitting width at 14 kbar. (d) Comparison between  $^{35}\text{Cl}$  NQR spin-lattice relaxation rate  $^{35}T_1^{-1}$  (red solid diamonds; left axis) and  $^{13}T_1^{-1}$  (blue open circles; right axis) under 14 kbar. The dotted line indicates the  $T^2$  law expected from the conventional phonons.

the soliton picture, is nothing but the binding transition of solitons. The jump of the order parameter at  $T_c$  is considered to indicate a sudden change from free-spin solitons to bound spin-soliton pairs with singlet-triplet excitations. Just below  $T_c$ , the spin-soliton binding may be so loose that each pair may sandwich minority domains, as shown in Fig. 1(d). On further cooling down to 200 K, the pairs become more strongly bound and eventually collapse at around 200 K, where the spin shift nearly vanishes. Concomitantly, the fraction of the minority domains fades out on cooling to 200 K, which reasonably explains the evolution of the order parameter. Superposed on this, the temperature variation of the polarization of the individual dimer should more or less contribute to the order parameter evolution.

$^{35}T_1^{-1}$ , which probes the lattice fluctuations through nuclear quadrupolar interaction, exhibits a divergent peak at  $T_c$  and decreases with temperature [Fig. 3(d)]. The peak in  $^{35}T_1^{-1}$ , in sharp contrast to its absence in  $^{13}T_1^{-1}$ , is attributable to the critical lattice fluctuations associated with the 3D ferroelectric dimerization transition and clearly indicates that  $^{35}T_1^{-1}$  probes quadrupole relaxation instead of magnetic relaxation through hyperfine interaction. This is consistent with the absolute value of  $^{35}T_1^{-1}$  that is too large to interpret in terms of the hyperfine interaction (see Appendix A for details).

At low temperatures below 140 K,  $^{35}T_1^{-1}$  is roughly proportional to  $T^2$ , suggesting the conventional phonon contribution (two-phonon Raman process) to the nuclear quadrupole relaxation [43]. Above 140 K, however, another relaxation contribution appears, and remarkably,  $^{35}T_1^{-1}$  and  $^{13}T_1^{-1}$  show the common temperature evolution for  $140 < T < 250$  K ( $< T_c$ ), indicating that the quadrupolar and magnetic relaxations have a common origin. This strongly indicates that the spin carriers are not conventional band quasiparticles but polarons, which travel with lattice distortion.

### C. Electrical resistivity

The electrical resistivity at 14 kbar is insulating below room temperature with a slight kink at  $T_c$  [Fig. 4(a)]; the activation energy of conductivity  $\sigma$  in the  $I_{\text{ferro}}$  phase is  $\Delta_\sigma \sim 2100$  K, which appears not to be much changed in the  $I_{\text{para}}$  phase [inset of Fig. 4(a)]. The band quasiparticle excitations would give a transport activation energy larger than half of the optical charge-transfer gap of  $\sim 0.7$  eV ( $\sim 8100$  K) in the ionic phase [15,44]. The substantially lower value of the observed charge excitation gap,  $2\Delta_\sigma \sim 4200$  K, suggests low-energy charge excitations distinct from the band quasiparticle excitations. Note that charge soliton excitations, which violate a 3D order, are prohibited in the  $I_{\text{ferro}}$  phase but are allowed when attaching themselves to spin solitons to form polarons, whose excitation energy should be reduced from that of the band quasiparticles due to lattice relaxation. This is the most likely case that explains the present observation. The rather smooth temperature variation of the electrical resistivity across  $T_c$  [Fig. 4(a)] indicates that the 3D long-range order of lattices does not largely affect the charge transport unlike in the spin excitations. This fact suggests that the sticking of spin solitons to charge solitons does not cause a large change in the charge excitation gap.

## IV. DISCUSSION

Consequently, there would be two types of spin excitations in the  $I_{\text{ferro}}$  phase: the triplet-type bound spin soliton pairs and the polaronic bound pairs of spin and charge solitons. In the  $I_{\text{para}}$  phase at room temperature and 14 kbar, the spin-soliton density was estimated at 1 per 10–25 donor-acceptor pairs by a previous NMR study [13]. On the other hand, a previous charge-transport study strongly suggested that the charge solitons reside in the  $I_{\text{para}}$  phase in that the resistivity in the  $I_{\text{para}}$  phase is a great deal smaller than that in the neutral phase [14]

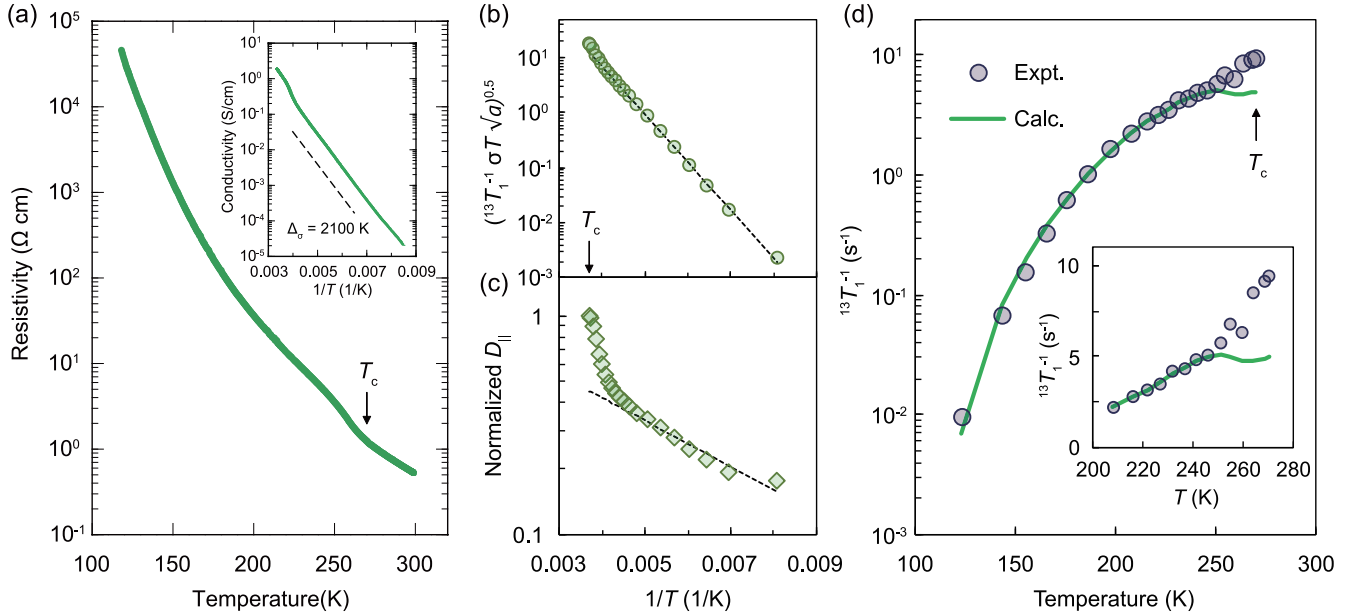


FIG. 4. Electrical resistivity of TTF-CA. (a) Temperature dependence of electrical resistivity at 14 kbar. Inset: Activation plot of electrical conductivity  $\sigma$ . The dotted line represents the Arrhenius form with an activation energy of 2100 K. (b) Plot of  $(^{13}T_1^{-1}\sigma T\sqrt{a})^{0.5}$ , which is proportional to the density of polarons  $n_p$  well below  $T_c$  (see text). The dotted line represents the Arrhenius form with an activation energy of 2010 K estimated using the data below 250 K. (c) Temperature dependence of the diffusion constant evaluated through Eq. (3) using  $\sigma$  and  $n_p$  (see text); the value at  $T_c$  is normalized to unity. The dotted line represents the Arrhenius form with an activation energy of 240 K estimated using the data below 220 K. (d) Comparison between the observed  $^{13}\text{C}$  NMR spin-lattice relaxation rate  $^{13}T_1^{-1}$  and the contribution of polarons to  $^{13}T_1^{-1}$ ,  $(^{13}T_1^{-1})_p$ , calculated using  $\sigma$  (see text).  $(^{13}T_1^{-1})_p$  is normalized to  $^{13}T_1^{-1}$  at 190 K. Inset: Behavior near  $T_c$  in linear scale. The excess in  $^{13}T_1^{-1}$  from the  $(^{13}T_1^{-1})_p$  curve near  $T_c$  is likely the contribution of the triplet excitations of the bound soliton pairs.

and that in the  $I_{\text{para}}$  phase of TTF-*p*-bromanil (TTF-BA), an ionic Mott insulator with strongly localized spins [45]. Here, we try to evaluate the charge-soliton density  $n_{\text{cs}}$  at 14 kbar in the  $I_{\text{para}}$  phase with reference to the density of neutral-ionic domain wall (NIDW)  $n_{\text{DW}}$  at  $\sim 9$  kbar in the NI crossover region and the pressure profile of conductivity  $\sigma$  at room temperature reported in Ref. [14].

A theoretical study suggests that, at the NI boundary where the neutral and ionic states are degenerate, the NI transition system can be mapped to the 1D Ising model, where the neutral (ionic) state corresponds to the up (down) spin and the NIDW is equivalent to a spinon [46]. According to this model,  $n_{\text{DW}}$  is given by  $n_{\text{DW}} \sim 1/2\xi$ , where the correlation length of the Ising model  $\xi$  roughly corresponds to half of the interspin distance, leading to one NIDW per about five donor-acceptor pairs at  $\sim 9$  kbar in the NI crossover region at room temperature [14]. When the system goes into the  $I_{\text{para}}$  phase, the neutral domains shrink down to a single neutral molecule sandwiched by a NIDW pair; that is the charge soliton as predicted in the theoretical studies [3,6] so that  $n_{\text{cs}} = n_{\text{DW}}/2$ . At room temperature, the  $\sigma$  value at  $\sim 9$  kbar decreases by one order with increasing pressure to 14 kbar [14], which suggests that the charge soliton (or NIDW pair) density  $n_{\text{cs}}$  is 1 per  $\sim 100$  donor-acceptor pairs at 14 kbar, assuming that the pressure dependence of  $\sigma$  at a fixed temperature is attributed to the charge carrier density. This value, much smaller than the spin-soliton density, is reasonable because, in the highly ionic phase, the excitation energy of the charge soliton (approximately the single neutral molecule) should be

larger than that of the spin soliton (approximately the single ionic molecule) [3,5,6].

Thus, the majority are the spin solitons at 14 kbar, suggesting that the magnetism just below  $T_c$  should be dominated by the bound spin solitons, whose triplet excitations with the large gap ( $\Delta_s$  of 3240 K) cause the steep decrease in spin shift. Well below  $T_c$ , where the triplet excitations almost vanish, polarons with lower excitation gaps ( $\Delta_{T_1^{-1}}$  of 1720 K in  $^{13}T_1^{-1}$  and  $\Delta_\sigma$  of 2100 K in  $\sigma$ ) would be the main contributors of magnetism and conductivity. The following analysis based on  $^{13}T_1^{-1}$  and  $\sigma$  gives further insight into the polaron formation.

Given that polarons move diffusively, their contribution to  $^{13}T_1^{-1}$ ,  $(^{13}T_1^{-1})_p$ , is expressed as (see Appendix B)

$$(^{13}T_1^{-1})_p \propto n_p / \sqrt{D_{\parallel}D_{\perp}}, \quad (1)$$

where  $n_p$  is the density of the polarons and  $D_{\parallel}$  ( $D_{\perp}$ ) is the diffusion constant of the polarons along the direction parallel (perpendicular) to the 1D chains. Equation (1) is rewritten in terms of the temperature-dependent anisotropy parameter,  $a(T) = D_{\perp}/D_{\parallel}$ , as

$$(^{13}T_1^{-1})_p \propto n_p / \sqrt{a}D_{\parallel}. \quad (2)$$

On the other hand,  $\sigma$  is expressed through the Einstein relation as

$$\sigma = n_p e^2 D_{\parallel} / k_B T, \quad (3)$$

where  $e$  is the elementary charge. Equations (2) and (3) yield  $n_p \propto [(^{13}T_1^{-1})_p \sigma T \sqrt{a}]^{0.5}$ , which is evaluated using the

experimental values of  $^{13}\text{T}_1^{-1}$  and  $\sigma$  and the conductivity anisotropy measuring the  $a$  values (see Appendix C). As shown in Fig. 4(b),  $n_p$  obeys  $n_p \propto \exp(-\Delta_n/k_B T)$  with  $\Delta_n \sim 2010$  K; a slight deviation of  $n_p$  from the activation line near  $T_c$  may be an artifact arising from the contribution of the bound spin solitons to  $^{13}\text{T}_1^{-1}$ . Applying the deduced activation form of  $n_p$  to the conductivity formula, Eq. (3), we obtain the temperature variation of  $D_{\parallel}$  as shown in Fig. 4(c). At low temperatures,  $D_{\parallel}$  shows an activation behavior indicating the thermal hopping over the energy barrier of 240 K caused by the lattice distortion due to the charge-lattice coupling. Remarkably, this energy scale is near the Peierls-coupled optical phonon frequencies of  $\sim 120$ – $180$  K in the  $I_{\text{ferro}}$  phase [47], suggesting that the polarons diffuse assisted by the Peierls phonon modes.  $D_{\parallel}$  goes up from the activation line upon approaching  $T_c$ , most likely because the reduction in the energy barrier just before the melting of the static dimerization near  $T_c$  promotes the diffusion of the carriers.

Then, substituting the obtained  $D_{\parallel}$  and the activation form of  $n_p$  in Eq. (2), we evaluate the polaron contribution to the relaxation rate  $(^{13}\text{T}_1^{-1})_p$ , which nearly coincides with the experimental  $^{13}\text{T}_1^{-1}$  values up to 250 K [Fig. 4(d)]. This suggests that the polaron motions are responsible for  $^{13}\text{T}_1^{-1}$  in  $120 < T < 250$  K; the deviation of the experimental  $^{13}\text{T}_1^{-1}$  values from  $(^{13}\text{T}_1^{-1})_p$  in  $250 \text{ K} < T < T_c$  is likely the contribution of the triplet excitations of the bound soliton pairs to  $^{13}\text{T}_1^{-1}$ . We also evaluate the polaron contribution to spin shift, assuming the activation form of  $n_p$  keeps holding for charge-soliton density  $n_{cs}$  in the  $I_{\text{para}}$  phase because of no clear break in the resistivity variation across  $T_c$  [Fig. 4(a)]. The known room-temperature value,  $n_{cs}(\text{RT})$ , of 1 per  $\sim 100$  donor-acceptor pairs determines the complete form of  $n_p(T)$ . Because a charge soliton is stuck by a spin soliton to form a polaron, the ratio of the polaron density  $n_p(T)$  to the room-temperature spin-soliton density  $n_{ss}(\text{RT})$ , 1 per 10–25 donor-acceptor pairs [13], gives the ratio of the polaron's contribution to the spin shift at  $T$  to the observed spin shift at room temperature as  $S_p(T)/S(\text{RT}) = [n_p(T)/n_{ss}(\text{RT})][\text{RT}/T]$ , assuming noninteracting spins. Thus calculated  $S_p(T)$  values are indicated by green lines in the inset of Fig. 2(b); they show that the triplets dominate the spin shift down to  $\sim 230$  K, below which the two contributions are comparable. This estimation is in agreement with the interpretation that the triplet contribution is captured in  $^{13}\text{T}_1^{-1}$  just below  $T_c$ .

Note that frozen domain walls are expected to emerge below  $T_c$  due to the multidomain structure in the ferroelectric; however, these domain walls are not mobile and thus do not affect the present findings related to the thermally activated mobile excitations.

## V. CONCLUSION

In the present work, we tackled the problem of how spin solitons and charge solitons vitally excited in a 1D polar dimer liquid conform to a 3D ferroelectric dimer order in a neutral-ionic transition system, TTF-CA. The NMR, NQR, and conductivity measurements all coherently point to a binding transition of the soliton matter to two-component composite pairings composed of neutral spin soliton pairs

and polaronic spin-soliton charge-soliton pairs. The spin soliton pairs contribute to magnetism through triplet excitations, which rapidly decrease upon cooling, whereas the polarons dominate the low-temperature magnetism and conductivity and diffusively travel with a hopping activation energy close to the Peierls-coupled optical phonon energies, suggestive of the Peierls phonon-assisted hopping. Solitons are mobile topological defects of keen interest and have been intensively explored, particularly in regard to their individual properties. The present work has revealed how solitons are organized when a system in the nonordered regime enters into the 3D symmetry-breaking ordered regime, offering a different perspective to soliton physics.

## ACKNOWLEDGMENTS

We thank H. Fukuyama for fruitful discussions. This work was supported by the JSPS Grants-in-Aid for Scientific Research (Grants No. JP16H06346, No. JP17K05532, No. JP18H05225, No. JP19H01846, and No. JP20K20894), by the Japan Science and Technology Agency, CREST (Grant No. JPMJCR1661), and by the Murata Science Foundation.

## APPENDIX A: HYPERFINE COUPLING CONSTANT OF $^{35}\text{Cl}$ NUCLEI IN THE CA MOLECULE

$T_1^{-1}$  is proportional to  $A^2\gamma_N^2$  for the magnetic relaxation, where  $A$  is the hyperfine coupling constant including both the isotropic and anisotropic parts and  $\gamma_N$  is the gyromagnetic ratio. As seen in Fig. 3(d),  $^{35}\text{T}_1^{-1}$  is  $\sim 100 \text{ s}^{-1}$ , and  $^{13}\text{T}_1^{-1} \sim 2 \text{ s}^{-1}$  at 200 K. The  $\gamma_N$  value of the  $^{35}\text{Cl}$  nucleus is  $^{35}\gamma_N/2\pi = 4.172 \text{ MHz/T}$  and that of the  $^{13}\text{C}$  nucleus is  $^{13}\gamma_N/2\pi = 10.705 \text{ MHz/T}$ . Thus, to attain  $^{35}\text{T}_1^{-1}$  of  $\sim 100 \text{ s}^{-1}$  by the magnetic relaxation,  $^{35}A$  needs to be about 18 times larger than  $^{13}A$ . However, the electron-density profiles of the HOMO of TTF [48] and the LUMO of CA [49], which are good references for seeing the relative magnitudes of the hyperfine fields, show that the electron density around the  $^{13}\text{C}$  site appears to be larger than that around the  $^{35}\text{Cl}$  site, implying  $^{13}A > ^{35}A$ . Therefore, the contribution of the magnetic relaxation in  $^{35}\text{T}_1^{-1}$  is expected to be much less than the observed value of  $^{13}\text{T}_1^{-1} \sim 2 \text{ s}^{-1}$ . This estimation strongly suggests that the origin of  $^{35}\text{T}_1^{-1}$  for  $140 < T < 250$  K is the quadrupolar interaction, not the hyperfine interaction. This consequence is corroborated by the fact the  $^{35}\text{T}_1^{-1}$  shows a sharp peak at  $T_c$ , while  $^{13}\text{T}_1^{-1}$  does not; namely,  $^{35}\text{T}_1^{-1}$  is caused by the quadrupole-coupled lattice fluctuations that are critically enhanced around  $T_c$ .

## APPENDIX B: NMR RELAXATION RATE DERIVED FROM DIFFUSIVE MOTIONS OF POLARONS

In the case that the relaxation of nuclear magnetization is caused by electron spins through hyperfine coupling tensors, the nuclear spin-lattice relaxation rate  $T_1^{-1}$  is expressed by [50,51]

$$T_1^{-1} = k_B T (\chi/N_A \mu_B^2) \gamma_N^2 [F_1 S(\omega_e) + F_2 S(\omega_N)], \quad (\text{B1})$$

where  $\chi$  is the spin susceptibility,  $\gamma_N$  is the nuclear gyromagnetic ratio,  $S(\omega)$  is the spectral density of electron

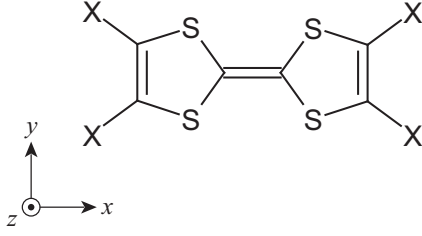


FIG. 5. Molecular principal axes of TTF ( $X = \text{H}$ ) and TMTTF ( $X = \text{CH}_3$ ) molecules.

spin fluctuations,  $\omega_e$  ( $\omega_N$ ) is the electron (nuclear) Larmor angular frequency,  $k_B$  is the Boltzmann constant,  $N_A$  is the Avogadro constant, and  $\mu_B$  is the Bohr magneton. The first (second) term is derived from the transverse (longitudinal) spin fluctuations. For the hyperfine coupling tensor with uniaxial symmetry,  $F_1$  and  $F_2$  are formulated as follows:

$$F_1 = \left[ a_{\text{iso}} + \frac{1}{2} a_{\text{aniso}} (1 - 3\cos^2\theta) \right]^2 + \frac{9}{4} a_{\text{aniso}}^2 \sin^4\theta \quad (\text{B2})$$

and

$$F_2 = \frac{9}{2} a_{\text{aniso}}^2 \sin^2\theta \cos^2\theta, \quad (\text{B3})$$

where  $a_{\text{iso}}$  ( $a_{\text{aniso}}$ ) is the isotropic (anisotropic) hyperfine coupling constant and  $\theta$  is the angle between the direction of the magnetic field  $H$  and the symmetry axis. The hyperfine coupling tensors of the central carbon sites in the TTF molecule are unknown for this compound, and thus, we used the tensor for the analogous materials  $(\text{TMTTF})_2X$  ( $X = \text{Br}$  and  $\text{AsF}_6$ ) reported in Ref. [13];  $a_{\text{iso}} = 3.6 \text{ kOe}/\mu_B$  [52], and  $(a_{\text{aniso}}^{xx}, a_{\text{aniso}}^{yy}, a_{\text{aniso}}^{zz}) = (-4.2, -5.3, 9.5) \text{ kOe}/\mu_B$  [53,54], where  $x$ ,  $y$ , and  $z$  are the molecular principal axes (see Fig. 5). The anisotropic part has a nearly uniaxial symmetry represented by  $(-a_{\text{aniso}}, -a_{\text{aniso}}, 2a_{\text{aniso}})$  with  $a_{\text{aniso}} \sim 4.7 \text{ kOe}/\mu_B$ . For the magnetic field orientation in the present study ( $H \parallel a$  axis),  $\theta$  is calculated to be  $24^\circ$  using the atomic coordinates determined by the neutron diffraction measurement [31]. These values yield  $F_1/F_2 \sim 0.1$ ; thus, the dominant term in  $T_1^{-1}$  is the second term, which describes electron spin fluctuations at  $\omega_N$  of 86 MHz, which is more than three orders of magnitude lower than  $\omega_e$  of the first term in the present experiments. When spins move diffusively along the 1D axis with a weak hopping in the perpendicular direction,  $S(\omega)$  is expressed by [55]

$$S(\omega) = \frac{1}{\sqrt{2D_{\parallel}D_{\perp}}} \left( \frac{1 + \sqrt{1 + (\omega/D_{\perp})^2}}{1 + (\omega/D_{\perp})^2} \right)^{1/2}, \quad (\text{B4})$$

where  $D_{\parallel}$  and  $D_{\perp}$  are the diffusion constants of spins along the directions parallel and perpendicular to the 1D axis. For

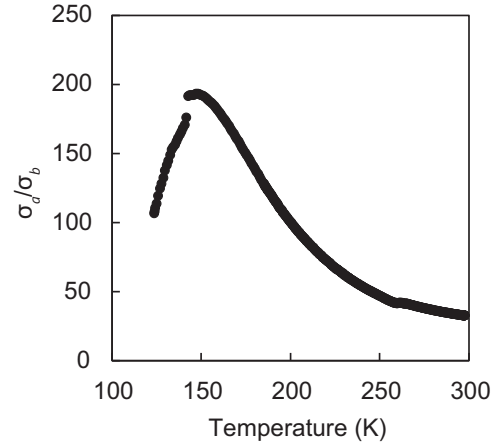


FIG. 6. Temperature dependence of the ratio of conductivities along the  $a$  and  $b$  axes  $\sigma_a/\sigma_b$  at 15 kbar.

$\omega \ll D_{\perp}$ ,  $S(\omega)$  is reduced to

$$S(\omega) = \frac{1}{\sqrt{D_{\parallel}D_{\perp}}}. \quad (\text{B5})$$

In the  $I_{\text{para}}$  phase at 14 kbar,  $D_{\parallel}$  and  $D_{\perp}$  of spin solitons are evaluated to be  $\sim 10^{11}$  and  $\sim 10^{10} \text{ s}^{-1}$  [13], respectively. On the other hand,  $\omega_N$  of the  $^{13}\text{C}$  nucleus is  $\sim 10^7 \text{ s}^{-1}$  at  $H = 8 \text{ T}$ ; thus,  $\omega_N \ll D_{\perp}$ . If the situation with  $\omega_N \ll D_{\perp}$  is appropriate for the polarons in the  $I_{\text{ferro}}$  phase, the contribution of polarons to  $^{13}\text{T}_1^{-1}$ ,  $(^{13}\text{T}_1^{-1})_{\text{p}}$ , is expressed by

$$(^{13}\text{T}_1^{-1})_{\text{p}} \sim k_B T (\chi_{\text{p}}/N_A \mu_B^2) \gamma_N^2 F_2 / \sqrt{D_{\parallel}D_{\perp}}, \quad (\text{B6})$$

where  $\chi_{\text{p}}$  is the spin susceptibility of polarons. Using the relation of  $n_{\text{p}} \propto T \chi_{\text{p}}$ ,  $(^{13}\text{T}_1^{-1})_{\text{p}}$  is rewritten as follows:

$$(^{13}\text{T}_1^{-1})_{\text{p}} \propto n_{\text{p}} / \sqrt{D_{\parallel}D_{\perp}}. \quad (\text{B7})$$

### APPENDIX C: ANISOTROPY OF DIFFUSION CONSTANTS

We used the ratio of conductivities along the  $a$  and  $b$  axes  $\sigma_b/\sigma_a$  at 15 kbar (Fig. 6) as the reference value of  $a(T) = D_{\perp}/D_{\parallel}$  at 14 kbar, where the  $a$  and  $b$  axes are the directions parallel and perpendicular to the 1D direction, respectively, because  $\sigma_{\parallel}(= \sigma_a)$  and  $\sigma_{\perp}(= \sigma_b)$  are expressed as

$$\sigma_{\parallel(\perp)} = n_{\text{p}} e^2 D_{\parallel(\perp)} / k_B T. \quad (\text{C1})$$

- [1] A. J. Heeger, S. Kivelson, J. R. Schrieffer, and W. P. Su, *Rev. Mod. Phys.* **60**, 781 (1988).  
 [2] S. Brazovskii, in *The Physics of Organic Superconductors and Conductors*, edited by A. Lebed, Springer Series in Materials Science Vol. 110 (Springer, Berlin, Heidelberg, 2008), pp. 313–355.  
 [3] N. Nagaosa, *J. Phys. Soc. Jpn.* **55**, 2754 (1986).

- [4] Z. G. Soos and A. Painelli, *Phys. Rev. B* **75**, 155119 (2007).  
 [5] H. Fukuyama and M. Ogata, *J. Phys. Soc. Jpn.* **85**, 023702 (2016).  
 [6] M. Tsuchiizu, H. Yoshioka, and H. Seo, *J. Phys. Soc. Jpn.* **85**, 104705 (2016).  
 [7] T. Mitani, G. Saito, Y. Tokura, and T. Koda, *Phys. Rev. Lett.* **53**, 842 (1984).

- [8] H. Okamoto, T. Mitani, Y. Tokura, S. Koshihara, T. Komatsu, Y. Iwasa, T. Koda, and G. Saito, *Phys. Rev. B* **43**, 8224 (1991).
- [9] T. Luty, H. Cailleau, S. Koshihara, E. Collet, M. Takesada, M. H. Lemée-Cailleau, M. Buron-Le Cointe, N. Nagaosa, Y. Tokura, E. Zienkiewicz, and B. Ouladdiaf, *Europhys. Lett.* **59**, 619 (2002).
- [10] M. Buron-Le Cointe, M. H. Lemée-Cailleau, H. Cailleau, S. Ravy, J. F. Bérrar, S. Rouzière, E. Elkaim, and E. Collet, *Phys. Rev. Lett.* **96**, 205503 (2006).
- [11] H. Kishida, H. Takamatsu, K. Fujinuma, and H. Okamoto, *Phys. Rev. B* **80**, 205201 (2009).
- [12] F. Kagawa, S. Horiuchi, H. Matsui, R. Kumai, Y. Onose, T. Hasegawa, and Y. Tokura, *Phys. Rev. Lett.* **104**, 227602 (2010).
- [13] K. Sunami, T. Nishikawa, K. Miyagawa, S. Horiuchi, R. Kato, T. Miyamoto, H. Okamoto, and K. Kanoda, *Sci. Adv.* **4**, eaau7725 (2018).
- [14] R. Takehara, K. Sunami, K. Miyagawa, T. Miyamoto, H. Okamoto, S. Horiuchi, R. Kato, and K. Kanoda, *Sci. Adv.* **5**, eaax8720 (2019).
- [15] J. B. Torrance, J. E. Vazquez, J. J. Mayerle, and V. Y. Lee, *Phys. Rev. Lett.* **46**, 253 (1981).
- [16] J. B. Torrance, A. Girlando, J. J. Mayerle, J. I. Crowley, V. Y. Lee, P. Batail, and S. J. LaPlaca, *Phys. Rev. Lett.* **47**, 1747 (1981).
- [17] M. Dressel and T. Peterseim, *Crystals* **7**, 17 (2017).
- [18] M. Masino, N. Castagnetti, and A. Girlando, *Crystals* **7**, 108 (2017).
- [19] G. D'Avino, A. Painelli, and Z. G. Soos, *Crystals* **7**, 144 (2017).
- [20] M. Buron-Le Cointe, E. Collet, B. Toudic, P. Czarnecki, and H. Cailleau, *Crystals* **7**, 285 (2017).
- [21] R. Takehara, K. Sunami, F. Iwase, M. Hosoda, K. Miyagawa, T. Miyamoto, H. Okamoto, and K. Kanoda, *Phys. Rev. B* **98**, 054103 (2018).
- [22] Y. Tokura, T. Koda, T. Mitani, and G. Saito, *Solid State Commun.* **43**, 757 (1982).
- [23] Y. Tokura, H. Okamoto, T. Koda, T. Mitani, and G. Saito, *Solid State Commun.* **57**, 607 (1986).
- [24] A. Girlando, C. Pecile, A. Brillante, and K. Syassen, *Solid State Commun.* **57**, 891 (1986).
- [25] S. Horiuchi, Y. Okimoto, R. Kumai, and Y. Tokura, *J. Phys. Soc. Jpn.* **69**, 1302 (2000).
- [26] H. Matsuzaki, H. Takamatsu, H. Kishida, and H. Okamoto, *J. Phys. Soc. Jpn.* **74**, 2925 (2005).
- [27] A. Dengl, R. Beyer, T. Peterseim, T. Ivek, G. Untereiner, and M. Dressel, *J. Chem. Phys.* **140**, 244511 (2014).
- [28] A. Girlando, F. Marzola, C. Pecile, and J. B. Torrance, *J. Chem. Phys.* **79**, 1075 (1983).
- [29] Y. Tokura, Y. Kaneko, H. Okamoto, S. Tanuma, T. Koda, T. Mitani, and G. Saito, *Mol. Cryst. Liq. Cryst.* **125**, 71 (1985).
- [30] A. Painelli and A. Girlando, *Phys. Rev. B* **37**, 5748 (1988).
- [31] M. Le Cointe, M. H. Lemée-Cailleau, H. Cailleau, B. Toudic, L. Toupet, G. Heger, F. Moussa, P. Schweiss, K. H. Kraft, and N. Karl, *Phys. Rev. B* **51**, 3374 (1995).
- [32] K. Kobayashi, S. Horiuchi, R. Kumai, F. Kagawa, Y. Murakami, and Y. Tokura, *Phys. Rev. Lett.* **108**, 237601 (2012).
- [33] M. H. Lemée-Cailleau, M. Le Cointe, H. Cailleau, T. Luty, F. Moussa, J. Roos, D. Brinkmann, B. Toudic, C. Ayache, and N. Karl, *Phys. Rev. Lett.* **79**, 1690 (1997).
- [34] J.-I. Kishine, T. Luty, and K. Yonemitsu, *Phys. Rev. B* **69**, 075115 (2004).
- [35] H. Okamoto, T. Koda, Y. Tokura, T. Mitani, and G. Saito, *Phys. Rev. B* **39**, 10693 (1989).
- [36] M. Masino, A. Girlando, and A. Brillante, *Phys. Rev. B* **76**, 064114 (2007).
- [37] P. Karpov and S. Brazovskii, *Phys. Rev. B* **94**, 125108 (2016).
- [38] E. Orignac and R. Chitra, *Phys. Rev. B* **70**, 214436 (2004).
- [39] Y. Itoh and H. Yasuoka, *J. Phys. Soc. Jpn.* **66**, 334 (1997).
- [40] E. Ehrenfreund and L. S. Smith, *Phys. Rev. B* **16**, 1870 (1977).
- [41] M. Gourdji, L. Guibé, A. Péneau, J. Gallier, B. Toudic, and H. Cailleau, *Solid State Commun.* **77**, 609 (1991).
- [42] J. Gallier, B. Toudic, Y. Delugeard, H. Cailleau, M. Gourdji, A. Péneau, and L. Guibé, *Phys. Rev. B* **47**, 11688 (1993).
- [43] A. Abragam, *The Principles of Nuclear Magnetism* (Oxford University Press, Oxford, 1961).
- [44] H. Okamoto, Y. Ishige, S. Tanaka, H. Kishida, S. Iwai, and Y. Tokura, *Phys. Rev. B* **70**, 165202 (2004).
- [45] K. Sunami, Y. Sakai, R. Takehara, H. Adachi, K. Miyagawa, S. Horiuchi, and K. Kanoda, *Phys. Rev. Res.* **2**, 043333 (2020).
- [46] R. Bruinsma, P. Bak, and J. B. Torrance, *Phys. Rev. B* **27**, 456 (1983).
- [47] M. Masino, A. Girlando, A. Brillante, R. G. Della Valle, E. Venuti, N. Drichko, and M. Dressel, *Chem. Phys.* **325**, 71 (2006).
- [48] C. Katan, *J. Phys. Chem. A* **103**, 1407 (1999).
- [49] V. Oison, C. Katan, and C. Koenig, *J. Phys. Chem. A* **105**, 4300 (2001).
- [50] F. Devreux, J.-P. Boucher, and M. Nechtschein, *J. Phys. (Paris)* **35**, 271 (1974).
- [51] M. Nechtschein, F. Devreux, R. L. Greene, T. C. Clarke, and G. B. Street, *Phys. Rev. Lett.* **44**, 356 (1980).
- [52] S. Fujiyama and T. Nakamura, *J. Phys. Soc. Jpn.* **75**, 014705 (2006).
- [53] E. Barthel, G. Quiron, P. Wzietek, D. Jerome, J. Christensen, and K. Bechgaard, *Europhys. Lett.* **21**, 87 (1993).
- [54] P. Delhaes, C. Coulon, J. Amiel, S. Flandrois, E. Toreilles, J. M. Fabre, and L. Giral, *Mol. Cryst. Liq. Cryst.* **50**, 43 (1979).
- [55] K. Mizoguchi, K. Kume, and H. Shirakawa, *Solid State Commun.* **50**, 213 (1984).